JCTC Journal of Chemical Theory and Computation

ARTICLE

pubs.acs.org/JCTC

Calculation of Hyperfine Tensors and Paramagnetic NMR Shifts Using the Relativistic Zeroth-Order Regular Approximation and Density Functional Theory

Jochen Autschbach,*[,†] Serguei Patchkovskii,[‡] and Ben Pritchard[†]

[†]Department of Chemistry, State University of New York at Buffalo, Buffalo, New York 14260-3000, United States

[‡]National Research Council of Canada, 100 Sussex Drive Ottawa, Ontario K1A 0R6, Canada

Supporting Information

ABSTRACT: Density functional theory (DFT) calculations of molecular hyperfine tensors were implemented as a second derivative property within the two-component relativistic zeroth-order regular approximation (ZORA). Hyperfine coupling constants were computed for systems ranging from light atomic radicals to molecules with heavy d and f block elements. For comparison, computations were also performed with a ZORA first-order derivative approach. In each set of computations, Slater-type basis sets have been used. The implementation allows for nonhybrid and hybrid DFT calculations and incorporates a Gaussian finite nucleus model. A comparison of results calculated with the PBE nonhybrid and the PBE0 hybrid functional is provided. Comparisons with differing basis sets and incorporation of finite-nucleus corrections are discussed. The second derivative method is applied to calculations of paramagnetic NMR ligand chemical shifts of three Ru(III) complexes. The results are consistent with those calculated using a first-order derivative method, and the results are consistent for different functionals used. A comparison of two different methods of calculating pseudo-contact shifts, one using the full hyperfine tensor and one assuming a point-charge paramagnetic center, is made for the Ru(III) complexes.

1. INTRODUCTION

Given a molecule with unpaired electrons in an external magnetic field $\boldsymbol{B}$, the interaction between the electrons, nuclei, and the external magnetic field can be described through the electron paramagnetic resonance (EPR) spin Hamiltonian:[1−4]

$$H_{\mathrm{spin}} = -\mathrm{g}\beta_e \mathbf{B}\cdot\mathbf{S} - g_N\beta_N \mathbf{B}\cdot\mathbf{I}_N - \mathbf{S}\cdot\mathbb{A}\mathbf{I}_N \qquad (1)$$

Here, g is the g-tensor (or g_e for a free electron) and g_N is the nuclear g-factor; $\mathbf{S}$ is the effective spin of the electronic system, and $\mathbf{I}_N$ is the nuclear spin operator. The first two terms in eq 1 are the electronic and nuclear Zeeman terms, describing the interaction between the electron and the external field, and between a nucleus and the external field, respectively. The final term is of interest to this work and describes the magnetic hyperfine interaction between the magnetic moments of the electron and the nuclei. The tensor $\mathbb{A}$ is the hyperfine coupling tensor. In order to compute the hyperfine tensor, it is necessary to consider three contributions: the "first-order" Fermi contact + spin−dipole (FC+SD) terms, and, in relativistic theories, a spin−orbit (SO) coupling cross term with the nuclear paramagnetic spin−orbital (PSO) operator (with the latter also being responsible for the paramagnetic NMR shielding in Ramsey's theory[5]). Details regarding the theory are provided in section 2, "Theoretical Methods". In nonrelativistic theory, the isotropic Fermi-contact term can be related to the excess (unpaired) spin density at a nucleus ($\rho^{\alpha-\beta}(0)$)[1,2,6] (assuming point nuclear charges, in atomic units where $\beta_e = 1/2$ and $\mu_0/(4\pi) = c^{-2}$):

$$A_{\mathrm{iso}}^{\mathrm{nrel}} = \left(\frac{4\pi}{6c^2}\right) g_e g_N \beta_N \langle S_z\rangle^{-1} \rho^{\alpha-\beta}(0) \qquad (2)$$

Here, $\rho^{\alpha-\beta}(0)$ is the excess spin density at the nucleus in question (the "contact" spin density). From eq 2, it can be seen that the value of A_{iso} may be positive or negative, depending on whether there exists an excess of α or β spin density at a particular nucleus. The sign of the hyperfine coupling constant is taken to be positive where the spins of the electron and nucleus are antiparallel.[1] In relativistic theories, the orbitals and the electron density have weak singularities at point nuclei, and the "contact" operators are modified accordingly in order to sample the electronic structure very close to, but not at, the nuclei.[7] The derivation in section 2 provides a case in point. The contact or near-contact nature of the relativistically generalized FC mechanism can generally be expected to be subject to large relativistic effects (scalar effects in particular). The anisotropic part of the hyperfine tensor is often not calculated because it does not contribute to the EPR hyperfine coupling for freely rotating molecules (for instance, in gas phase or solution). However, it is an important ingredient for calculations of paramagnetic NMR (pNMR) pseudo-contact chemical shifts.[8] In pNMR, large A_{iso} further give rise to sizable contact shifts.[8,9] The spin−orbit contribution to the hyperfine tensor is often neglected for light atomic systems, but it becomes increasingly important with increasing atomic number.[10] Inclusion or neglect of scalar relativistic and spin−orbit (SO) effects can greatly affect the value of magnetic properties, including hyperfine tensors, due to the requirement of describing electrons in close proximity to the nucleus and therefore exhibiting

Received: February 25, 2011
Published: June 06, 2011

relativistic behavior. Arbuznikov et al. have investigated spin−orbit effects on hyperfine tensors and found that the effects can be very significant for a range of molecules and nuclei.[10] In general, it was found that the correlation to experiment improved when SO terms were included in the calculation of the hyperfine tensor.

The treatment of SO effects in calculations of hyperfine coupling tensors may be assigned to one of two types. These two approaches mirror those previously discussed by us in a paper on calculating electronic *g*-tensors[11] and, therefore, are only briefly summarized described here. In the first type of calculation, SO coupling is included variationally in the ground state. The hyperfine tensor is then calculated as a first-order derivative of the energy; therefore, this route may be termed the "first-order" or "expectation value" (EV) approach, and has been implemented in the framework of the two-component relativistic zeroth-order regular approximation (ZORA)[12] by van Lenthe, van der Avoird, and Wormer.[13] The method has been successfully applied in conjunction with density functional theory (DFT) to transition-metal complexes and small organic molecules.[13]

Alternatively, SO coupling can be introduced as a perturbation on top of nonrelativistic or scalar-relativistic calculations. In this case, the hyperfine tensor is calculated from double-perturbation theory as a second derivative of energy with respect to the nuclear spin angular momentum and the effective electronic spin. The SO contributions to the hyperfine tensor are calculated to lowest order in this approach from solving a set of linear response equations, while the FC+SD terms are still computed from an expectation value integral involving the ground-state orbitals/wave function only. This type of calculation may be termed the "second-order" or "linear response" (LR) approach. One purpose of this article is to present an implementation and first application of the LR approach in conjunction with the ZORA formalism in the calculation of hyperfine tensors and hyperfine coupling constants. The approach presented here closely follows a recent development of a ZORA-based LR method for density functional theory (DFT) calculations of electronic *g*-tensors.[11]

DFT is an attractive electronic structure for calculating many molecular properties because of its relatively low computational expense and its often acceptable-to-good accuracy. DFT been used previously for calculations of magnetic properties of open-shell molecules.[6,10,14,15] Calculations of hyperfine tensors and, in particular, isotropic hyperfine coupling constants, have been previously carried out and benchmarked by various groups using DFT. Hermosilla et al. have analyzed a set of organic and inorganic radicals with the B3LYP hybrid functional and several basis sets, concluding through the use of regression analysis, that such a computational approach is appropriate.[16,17] Later, Barone et al. calculated hyperfine tensors for 208 free radicals using the B3LYP hybrid functional, again deeming the functional suitable.[14] It should be noted that, in these studies, relativistic effects were not included since they are likely unimportant for the relatively light atoms studied. Compounds with heavier nuclei (in particular, transition-metal complexes) have been studied by a number of authors, in some cases including SO effects[18−20] and with relativistic effects included using a second-order approach.[10]

Herein, we investigate the performance of a LR method of calculating hyperfine tensors using DFT and the two-component relativistic ZORA Hamiltonian. The new implementation allows one to directly compare results calculated with this method to those calculated with the aforementioned EV method reported by van Lenthe et al.[13] Differences may be expected for molecules where SO coupling is large, such as radicals with third-row transition metals, lanthanides, or actinides. Both our new LR method and the EV method of van Lenthe et al.[13] are implemented in the Amsterdam Density Functional (ADF) package,[21] which is a DFT code that makes use of Slater-type orbital (STO) basis sets. There are several reasons why it is desirable to have a relativistic LR approach available for hyperfine tensor computations. First, in terms of computational efficiency, variational SO DFT computations for large molecules can become very demanding on the computational resources, whereas the LR approach has a computational cost that is comparable to that of scalar relativistic ground-state computations with real orbitals. For systems with light to intermediate strength of SO effects, the analytic LR approach may also be advantageous in terms of numerical accuracy. Another reason pertains the prediction of the absolute and relative signs of the *g*- and the hyperfine tensors; the sign, which is important for pNMR applications, is straightforwardly determined in LR calculations. In our recent work on *g*-tensors, we have highlighted an example (NpF_6) where the prediction of the sign of a tensor appears to be problematic. We note that the new LR implementation is capable of handling hybrid functionals and it incorporates finite nucleus effects, which can be significant for hyperfine coupling tensors of heavy atoms.[20]

After presenting the theoretical background (section 2) and some details regarding the computations (section 3, "Computational Details"), the results of computations using the LR ZORA DFT implementation and other methods are compared in section 4.1, in "Results and Discussion", using a test set of small molecules with light and heavy atoms. Comparisons are also made with previously calculated values and with experiment, where available. Effects due to basis set, functional (nonhybrid vs hybrid), and finite nucleus corrections are investigated in some detail. We find that the LR method performs well in comparison with the EV method, even for systems with very heavy atoms. For heavy-nucleus hyperfine couplings, finite nucleus effects can be substantial. The sensitivity of hyperfine couplings to features of the electronic structure near the nuclei highlights the need for augmentation of the basis set with high exponent functions (in particular, in relativistic computations). As an additional application, calculated pNMR contact and pseudo-contact shifts are reported for three Ru(III) complexes (see section 4.2). These and several other complexes have been used recently for a computational pNMR benchmark by Rastrelli and Bagno.[9,22] In ref 22, relativistic effects on the ligand contact shifts were considered using the EV ZORA implementation of ADF, in conjunction with nonhybrid functionals, whereas the influence of the functional has been assessed by a comparison with nonrelativistic B3LYP LR calculations, using Gaussian-type basis sets. We take the opportunity here to revisit a subset of the complexes studied by Rastrelli and Bagno for which the new LR code allows us to investigate the performance of various functionals consistently within the ZORA LR regime using the same STO basis sets. For the pseudo-contact shifts, a comparison is made between using equations for the dipolar interaction, assuming a point paramagnetic center and using the dipolar hyperfine and *g*-tensors calculated from DFT.

2. THEORETICAL METHODS

2.1. Hyperfine Tensors Calculated As Second Derivatives of the Scalar Relativistic Electronic Energy. What follows is a

brief outline of the theory as it applies to hyperfine tensors. For a related ZORA-based derivation for LR calculations of *g*-tensors providing additional details and references, we refer the reader to ref 11. If spin−orbit (SO) effects are to be treated as a perturbation, element u,v of the hyperfine coupling tensor with $u,v \in \{x, y, z\}$ can be defined as a second derivative of energy, with respect to electron and nuclear spin:

$$A_{uv} = \frac{\partial^2 E}{\partial I_u \partial S_v} = g_N \beta_N \frac{\partial^2 E}{\partial \mu_{N,u} \partial S_v} \tag{3}$$

Here, and in the following, derivatives are assumed to be taken at $I_u = 0$, to eliminate higher-order terms from the nuclear spin perturbation. Assuming either a complete basis set or a basis set that is not dependent on the derivative parameters (which is the case for hyperfine coupling), the hyperfine tensor components for nucleus N are within a spin-unrestricted Kohn−Sham DFT, which is given as follows: The "first-order" (EV) FC+SD term reads

$$A_{uv}^{\mathrm{FC+SD}} = \frac{2 g_N \beta_N}{n_\alpha - n_\beta} \sum_{r,s} P_{sr}^{(0)\alpha-\beta} \langle \chi_r | \hat{h}^{(u,v)} | \chi_s \rangle \tag{4a}$$

and the second-order (linear response) paramagnetic spin orbital−spin orbit (PSOSO) term is given as

$$A_{uv}^{\mathrm{PSOSO}} = \frac{2 g_N \beta_N}{n_\alpha - n_\beta} \sum_{r,s} P_{sr}^{(v)\alpha-\beta} \langle \chi_r | \hat{h}^{(u)} | \chi_s \rangle \tag{4b}$$

Here, n_α and n_β are the numbers of occupied α and β spin orbitals, respectively, expressed in the basis set $\{\chi_r\}$ with MO coefficients $C_{ri}^{(0)}$ (unperturbed) and $C_{ri}^{(v)}$ (perturbed by the v component of the nuclear spin magnetic moment or by the v component of the SO operator derivative with respect to the electron spin operator). Furthermore, $P_{rs}^{(0)\alpha-\beta}$ and $P_{rs}^{(v)\alpha-\beta}$ are elements of the scalar relativistic unperturbed and first-order spin density matrices:

$$P_{rs}^{(0)\alpha-\beta} = \sum_i n_i^\alpha C_{ri}^{(0)\alpha} C_{si}^{*(0)\alpha} - \sum_i n_i^\beta C_{ri}^{(0)\beta} C_{si}^{*(0)\beta} \tag{5a}$$

$$P_{rs}^{(v)\alpha-\beta} = \sum_i n_i^\alpha [C_{ri}^{(0)\alpha} C_{si}^{*(v)\alpha} + C_{ri}^{(v)\alpha} C_{si}^{*(0)\alpha}] - \sum_i n_i^\beta [C_{ri}^{(0)\beta} C_{si}^{*(v)\beta} + C_{ri}^{(v)\beta} C_{si}^{*(0)\beta}] \tag{5b}$$

The ZORA[12] one-electron Fock operator in the absence of electromagnetic fields used in DFT computations with a local effective potential V reads (in atomic units)

$$\hat{h} = V + \frac{1}{2}(\vec{\sigma}\cdot\hat{\mathbf{p}})\mathscr{K}(\vec{\sigma}\cdot\hat{\mathbf{p}}) = V + \frac{1}{2}\hat{\mathbf{p}}\mathscr{K}\hat{\mathbf{p}} + \frac{1}{2}\imath\vec{\sigma}\cdot(\hat{\mathbf{p}}\mathscr{K}\times\hat{\mathbf{p}}) \tag{6}$$

with

$$\mathscr{K} = \frac{2c^2}{2c^2 - V} \tag{7}$$

The potential in $\mathscr{K}$ is typically approximated by a sum of local atomic potentials, which represents an efficient but quite accurate approximation of ZORA used in several electronic structure program packages.[23−26] In a hybrid DFT scheme, part of the effective exchange potential in eq 6 may be combined with a fraction of Hartree−Fock exchange. In eq 6, $\vec{\sigma}$ is the 3-vector of 2 × 2 Pauli spin matrices, with components $\vec{\sigma} = (\sigma_x, \sigma_y, \sigma_z)$, and $\hat{\mathbf{p}} = -i\boldsymbol{\nabla}$ is the momentum vector operator. Regarding the importance of two-electron SO terms see refs 11 and 27. The scalar relativistic part of eq 6 is taken to be the zeroth-order Fock operator,

$$\hat{h}^{(0)} = V + \frac{1}{2}\hat{\mathbf{p}}\mathscr{K}\hat{\mathbf{p}} \tag{8}$$

while the last term on the right-hand side of eq 6, the ZORA SO operator, is considered to be one of the perturbations. The nuclear spin magnetic perturbation is included in the formalism, following the derivations of refs 11, 13, and 28. The relevant perturbation operators to calculate hyperfine tensors for point nuclei are given by

$$\hat{h}^{(u)} = -\frac{i}{2}[\mathscr{K}(\mathbf{U}_N \times \boldsymbol{\nabla})_u + (\mathbf{U}_N \times \boldsymbol{\nabla})_u \mathscr{K}] \tag{9a}$$

$$\hat{h}^{(v)} = \frac{i}{2}(\hat{\mathbf{p}}\mathscr{K}\times\hat{\mathbf{p}})_v \tag{9b}$$

$$\hat{h}^{(u,v)} = \frac{1}{2}\{\delta_{uv}\boldsymbol{\nabla}\cdot(\mathscr{K}\mathbf{U}_N) - \boldsymbol{\nabla}_u(\mathscr{K}\mathbf{U}_{N,v})\} \tag{9c}$$

In the previous equations,

$$\mathbf{U}_N = c^{-2}\left(\frac{\mathbf{r}_N}{{r_N}^3}\right) \tag{10}$$

assuming a nuclear point magnetic dipole. Here, $\mathbf{r}_N$ is the electron−nucleus distance vector and r_N is its length. (For incorporation of a finite nucleus model, see below.) The operator in eq 9c is the sum of the ZORA analogs of the FC+SD operator derivatives, and eq 9a is the paramagnetic spin−orbit (PSO) operator. Regarding eq 9c, it is important to keep in mind that the derivations leading to the operators as published in refs 28 and 29 implicate that $\boldsymbol{\nabla}$ in this operator only acts inside the operator, not on any function to the right-hand side of the expression. To indicate this, the operator has been enclosed between curly brackets $\{\cdots\}$. The operator in eq 9b does not occur explicitly in eqs 4a and 4b. It is used to calculate the perturbed MO coefficients and density matrices (eq 5b) using methods to solve the coupled-perturbed Kohn−Sham (CPKS) equations that have been described elsewhere.[29−31] We have also implemented the LR part of the computations with the reverse order of perturbation operators, i.e. by solving the CPKS equations for the perturbation eq 9a for each nucleus, instead of using eq 9b, and obtained identical results as required by the interchange theorem of double perturbation theory.

2.2. Nonrelativistic Limit, Pauli Approximation, and Point-Charge Models. The nonrelativistic limit within the ZORA framework is given by $\mathscr{K} \to 1$. In this case, the hyperfine tensor has only the EV contribution, because the spin derivative of the SO operator ($\hat{h}^{(v)}$) vanishes. If the hyperfine tensor is calculated by using the Pauli approximation of the SO operator, the operator of eq 9b approximates to

$$\hat{h}^{(v)}(\mathrm{Pauli}) = \frac{i}{4c^2}(\hat{\mathbf{p}}V\times\hat{\mathbf{p}})_v \tag{11}$$

corresponding to the substitution $\mathscr{K} \to V/(2c^2)$. Schreckenbach and Ziegler[32] used the operator that is described by eq 11 for LR calculations of molecular *g*-tensors based on the Pauli approximation. For LR calculations of *g*-tensors, the SO "spin perturbation" yielding the operator $\hat{h}^{(v)}$ is the same as that used in the calculations of hyperfine tensors.

The nonrelativistic limit of the operator $\hat{h}^{(u)}$ in eq 9a is the well-known PSO operator that is used to calculate nonrelativistic nuclear magnetic shielding and J-coupling tensors. The factor of $1/c^2$ in this operator indicates the smallness of nuclear hyperfine terms and corresponds to $\mu_0/(4\pi)$ in SI units converted to atomic units. Threfore, this factor is not altered when taking a $c \rightarrow \infty$ nonrelativistic limit.

The nonrelativistic limit of the FC+SD operator derivative is obtained with the help of

$$\nabla_u \left(\frac{\mathbf{r}_N}{{r_N}^3}\right) = \left(\frac{4\pi}{3}\right)\delta_{uv}\delta(\mathbf{r}_N) + \frac{\delta_{uv}}{{r_N}^3} - 3\left(\frac{r_{N,u}r_{N,v}}{{r_N}^5}\right)$$

After letting $\mathscr{K} \rightarrow 1$, taking the derivatives of $\mathbf{U}_N$ in eq 9c, and regrouping terms, the operator reads

$$\hat{h}^{(u,v)}(\mathrm{nrel}) = \frac{1}{2c^2}\left(\left(\frac{8\pi}{3}\right)\delta_{uv}\delta(\mathbf{r}_N) - \left[\frac{\delta_{uv}}{{r_N}^3} - 3\left(\frac{r_{N,u}r_{N,v}}{{r_N}^5}\right)\right]\right) \quad (12)$$

Using this operator in the first term on the rhs of eq 4a yields an expression that is equivalent to the hyperfine tensor contributions given in eqs 2 and 3 of Eriksson,[2] apart from a factor of $g_e\beta_e$, which equals 1 in atomic units used here, and a factor of c^{-2} that is not present in Eriksson's equation. This factor, again originating from $\mu_0/(4\pi)$ in SI units, indicates the smallness of the nuclear hyperfine terms, relative to other perturbations.

Consider a situation where the hyperfine interaction is caused by one singly occupied molecular orbital (SOMO), with all α orbitals, for the sake of simplicity, assumed to have the same shape as their β counterparts, and $n_\alpha - n_\beta = 1$ in eqs 4a and 4b. In this case, the density matrices in eqs 5a and 5b are both reduced to one term from the SOMO. The assumption that the SOMO is completely localized on one paramagnetic center (for example, a heavy metal) located at the coordinate origin leads to a purely dipolar "through space" hyperfine tensor. Approximating the SOMO spin density as a delta distribution (a point spin density) simplifies the nonrelativistic EV in eq 4a to

$$A^{\mathrm{dip}}_{u,v}(\mathrm{nrel}) \approx \frac{g_N\beta_N}{c^2}\left[3\left(\frac{r_{N,u}r_{N,v}}{{r_N}^5}\right) - \frac{\delta_{uv}}{{r_N}^3}\right] \quad (13)$$

(in atomic units). This simplification is commonly applied in calculations of pseudo-contact (PC) shifts.[33]

2.3. Calculation of Operator Matrix Elements, Finite Nucleus Model. The perturbation operators for hyperfine coupling and g-factors, such as other magnetic perturbation operators in ZORA, involve derivatives of $\mathscr{K}$. In numerical integrations, it is desirable to avoid the calculation of these derivatives. By using the turnover rule for the momentum operator and/or partial integration, the derivatives can be switched over to the basis functions χ_μ and χ_ν instead, assuming that the basis functions vanish at the integration limits.

For the PSO operator (eq 9a) needed for hyperfine coupling, the AO matrix elements are the same as those reported in ref 29, which read as follows (after partial integration):

$$h^{(u)}_{rs} = -\frac{i}{2}\int \mathrm{d}^3r \cdot \mathscr{K}(\mathbf{U}_N \times [\chi_r^*(\boldsymbol{\nabla}\chi_s) - (\boldsymbol{\nabla}\chi_r^*)\chi_s])_u \quad (14)$$

To calculate the analogous matrix elements needed for g-tensors, one simply replaces $\mathbf{U}_N$ by $\mathbf{r}/2$, as outlined in ref 11. In some of the calculations, we have adopted a finite nucleus model in the form of Gaussian nuclear charge distributions.[34,35] In this case, the nuclear charge density is given as

$$\rho_N^{\mathrm{Gauss}}(\mathbf{R}) = Z_N\left(\frac{\xi_N}{\pi}\right)^{3/2}\exp\left(-\xi_N|\mathbf{R}-\mathbf{R}_N|^2\right) \quad (15)$$

where $\boldsymbol{R}_N$ is the charge center of nucleus N and $\mathbf{R}$ is a position in space where the nuclear charge density is evaluated. The exponent ξ_N is readily calculated from the nuclear isotope mass.[34] We define $\tilde{r}_N = (\xi_N)^{1/2}r_N$. With the finite nucleus model, the matrix elements of the PSO operator can be straightforwardly calculated from

$$h^{(u)}_{rs} = -\frac{i}{2}\int \mathrm{d}^3r \cdot \mathscr{K}P\left(\frac{3}{2},\tilde{r}_N^2\right)(\mathbf{U}_N \times [\chi_r^*(\boldsymbol{\nabla}\chi_s) - (\boldsymbol{\nabla}\chi_r^*)\chi_s])_u \quad (16)$$

where $P(a,x)$ is the lower incomplete gamma function ratio:

$$P(a,x) = \frac{1}{\Gamma(a)}\int_0^x \mathrm{d}t\, t^{a-1}\exp(-t) \quad (17)$$

For a point nucleus, the value of $P(3/2,\tilde{r}_N^2)$ in eq 16 is equal to 1 and eq 14 is recovered. The adoption of a Gaussian nucleus model in other hyperfine integrals leads to the same substitution of $\mathscr{K}\mathbf{U}_N$ by $\mathscr{K}P(3/2,\tilde{r}_N^2)\mathbf{U}_N$, which we therefore adopt in the following. Furthermore, the potential energy terms used to determine $\mathscr{K}$ in eq 7 and the electron−nucleus potential used in $\hat{h}^{(0)}$ are calculated based on the Gaussian nucleus model. For further details (presented in the context of calculations of nuclear indirect spin−spin coupling), please see ref 31.

For the bilinear FC+SD operator in eq 9c, the derivatives are only acting within the operator. Thus, a simple partial integration shifts the derivative to the product of the basis functions instead:

$$h^{(u,v)}_{rs} = -\frac{1}{2}\delta_{uv}\int \mathrm{d}^3r\mathscr{K}P\left(\frac{3}{2},\tilde{r}_N^2\right)\mathbf{U}_N \cdot \boldsymbol{\nabla}(\chi_r^*\chi_s) + \frac{1}{2}\int \mathrm{d}^3r\mathscr{K}P\left(\frac{3}{2},\tilde{r}_N^2\right)\mathrm{U}_{N,v}\boldsymbol{\nabla}_u(\chi_r^*\chi_s) \quad (18)$$

For the matrix elements of the spin−orbit operator derivative $\hat{h}^{(v)}$, we have adopted the same technique that was used for our recent development for g-tensor computations. The relevant AO integrals are calculated numerically using

$$h^{(v)}_{\mu\nu} = \frac{i}{2}\int \mathrm{d}^3r(\mathscr{K}-1)[\{\boldsymbol{\nabla}\chi_\mu^*\} \times \{\boldsymbol{\nabla}\chi_\nu\}] \quad (19)$$

As for the other operator matrix elements, with the Gaussian nucleus model, the function $\mathscr{K}$ used in the numerical integration is not the same as when a point nucleus model is adopted.

3. COMPUTATIONAL DETAILS

All computations were carried out with a developers version (pre-2010 release) of the Amsterdam Density Functional (ADF) package.[21] Geometry optimizations of the molecules in the test set employed the BP86 functional[36−38] and a triple-zeta polarized STO all-electron basis set with two sets of polarization functions for all atoms (TZ2P from the ADF basis set library), and the scalar ZORA spin-unrestricted formalism. The small molecule test set is a subset of that used in our recent benchmark of ZORA g-tensor calculations.[11] Point-group symmetry was not explicitly applied in the computations. Calculations of the

hyperfine tensors were based on the optimized geometries and employed a setting of 7.0 for the numerical integration accuracy parameter to ensure well-converged results and accurate perturbation operator integrals.

The functionals used in the hyperfine-tensor calculations were the Perdew−Burke−Ernzerhof (PBE) nonhybrid functional and, for comparison, the PBE-based PBE0 hybrid functional,[39,40] which affords 25% Hartree−Fock exchange. In the calculation of hyperfine tensors, a basis set that includes high-exponent functions must be used to accurately calculate the Fermi-contact term.[41] Therefore, a custom STO basis set (JCPL) was used, based on previous work on nuclear spin−spin coupling.[42,43] This basis set includes functions with high exponents that are required to model the electronic structure close to the nucleus. To determine the effect of the point-nuclei approximation, calculations using a Gaussian finite-nucleus correction were carried out with HgH, HgF, and NpF_6, using the implementation in ref 31, and as outlined above. The comparison between the LR method outlined in Section 2 and the EV approach made use of the ADF implementation by van Lenthe et al.[13] For comparison, computations with both codes were performed with spin-unrestricted scalar ZORA orbitals, as well as with spin-restricted orbitals populated using configurations with $n_\alpha \neq n_\beta$.

The structures of Ru(III) complexes chosen for comparison with the work of Rastrelli and Bagno[22] were optimized according to the procedure outlined by Rastrelli and Bagno, which is almost identical to that detailed above (BP86/TZ2P, no symmetry, spin-unrestricted scalar ZORA).[22] Hyperfine calculations were then carried out as previously described, and also with the Becke88−Perdew86 (BP) nonhybrid functional and with the popular Becke three-parameter hybrid B3LYP.[44] In order to save some computational expense, the JCPL basis was used solely for the hydrogen atoms for these three molecules; the regular ZORA-optimized TZ2P basis from the ADF basis set library was used for all other atoms. Since the valence basis functions in JCPL are derived from TZ2P, the use of this locally dense basis is not expected to lead to a basis set imbalance for the Ru(III) complexes.

When calculating properties using basis sets as large as JCPL used in the current study, near-linear dependencies may form in the basis set. Overcompleteness of the AO basis can be remedied by removing problematic linear combinations of the basis functions. Such a case occurred with some of the molecules when using the hybrid functionals (PBE0 and B3LYP), in which case a check for linear dependency is automatically switched on in the ADF program. Some molecular orbitals (MOs) were removed accordingly from the self-consistent field procedure and from the MO set used in the calculation of the magnetic properties in order to reduce numerical noise.

4. RESULTS AND DISCUSSION

4.1. Hyperfine Coupling: General Performance of the LR ZORA Approach, Basis Set Effects, and Finite Nucleus Corrections. A summary of the results of the calculation for the suite of test molecules using the various approaches is shown in Table 1. Most results are given with four significant figures; some small numbers are given to within 3 decimal places. Very small values may be affected by the numerical precision of the calculation. All hyperfine couplings are given in SI units of MHz. These can be converted to units of Gauss (G), using the following formula:[3]

$$A_{\mathrm{MHz}} = 2.8025\left(\frac{g_{\mathrm{iso}}}{g_{\mathrm{e}}}\right)A_{\mathrm{Gauss}} \qquad (20)$$

where g_{iso} is the isotropic g-factor (LR data consistent with the hyperfine couplings may be taken from ref 11), and g_e is the free-electron g-value. Electron paramagnetic resonance (EPR) experiments cannot straightforwardly deduce the sign of the isotropic hyperfine coupling; therefore, the sign of the experimental hyperfine coupling has been listed in agreement with the sign predicted by the computations.

There is excellent agreement between the method developed in this study and the EV method of van Lenthe et al. for atoms in the first to third rows. For the heavier elements (e.g., Hg), the agreement is still very close, although it can be seen that, percentage-wise, there are significant differences in the PSOSO mechanism for these linear molecules. A breakdown of the perturbational treatment of the SO operator for linear systems echoes that for g-tensors; for a detailed discussion and further references, we refer the reader to refs 11, 54, and 55 . The overall good agreement between the LR and EV treatment of hyperfine coupling is not surprising, since the hyperfine tensor has large nonrelativistic and scalar relativistic contributions, which are calculated to be the same with both methods.

In the spin-restricted calculations, we have calculated the FC+SD and the PSOSO terms obtained from the first-order EV approach separately. When comparing these results to those from the spin-restricted LR calculations, it is apparent that for light atomic systems where SO coupling is small, the two mechanisms yield essentially identical results. Continuing with the comparison of the spin-restricted results, starting with SiOH and SiSH, one begins to observe small deviations in the dominating FC+SD term between the two approaches, which is due to SO coupling slightly affecting the shape of the ground-state unperturbed MOs in the EV computations. The PSOSO mechanism also begins to exhibit some differences; we remind the reader that, in the EV approach, this contribution is calculated from an expectation value, just like the FC+SD mechanism, whereas in the LR approach the PSOSO contribution is calculated from the linear response of the orbitals to either the PSO or the SO operator (see section 2).

Larger deviations between calculations and experiment are found for the hyperfine coupling constant of the neptunium nucleus of NpF_6, with the first-order spin-polarized EV treatment underestimating the isotropic coupling and the LR spin-polarized treatment overestimating the isotropic coupling. The spin-restricted calculations are clearly not suitable at all for this coupling constant. Sizable deviations also occur for the fluorine nuclei in HgF, TiF_3, and NpF_6, with both the LR and EV methods underestimating the magnitude of the experimental isotropic hyperfine value. This underestimation is often correlated with the number of lone pairs on the atom of interest and the deficiency of commonly used (LDA and GGA, but also hybrid) functionals in accurately modeling the spin densities with nuclei-containing multiple lone electron pairs.[10,56,57]

The effect of SO coupling is explicitly (separately) obtained in the set of LR data. While this effect generally small for first- and second-row elements, the need for SO treatment increases with increasing atomic number. Where the SO term is large (in HgH and NpF_6), its inclusion substantially improves the results, compared to a method neglecting this effect. Indeed, for the

Table 1. Summary of Calculated and Experimental Isotropic Hyperfine Coupling Constants (All Values Given in MHz)[a]

	Spin-Polarized LR[b] (PBE)			Spin-Polarized LR[b] (PBE0)			Spin-Restricted LR[b] (PBE)			Spin-Polarized	Spin-Restricted EV[c]				
	FC+SD	PSOSO	total	FC+SD	PSOSO	total	FC+SD	PSOSO	total	EV	FC+SD	PSOSO	total	exp.	previous calc.
CH_2															
C	208.3	−0.180	208.2	223.7	−0.180	223.5	133.5	−0.153	133.4	209.1					
H	−19.39	0.009	−19.38	−25.51	0.009	−25.50	39.66	0.010	39.67	−19.43					
CH_3															
C	66.64	−0.152	66.49	82.05	−0.157	81.89	0.071	−0.100	−0.029	67.02	0.070	−0.100	−0.029	108[d]	
H	−65.47	0.018	−65.45	−74.20	0.017	−74.19	0.002	0.022	0.024	−65.44	0.001	0.022	0.024	−64.46[d]	
HCO															
C	385.4	−0.478	384.9	393.4	−0.495	392.9	367.0	−0.581	366.4	386.8	367.0	−0.591	366.4	365[e]	
H	375.6	−0.083	375.5	378.5	−0.084	378.5	334.6	−0.109	334.5	375.2	334.6	−0.119	334.5	354[e]	343.1[k]
O	−22.11	0.490	−21.62	−32.21	0.468	−31.74	−13.95	0.538	−13.41	−21.72	−13.95	0.540	−13.41		
HSiO															
Si	−541.8	0.878	−540.9	−557.4	0.859	−556.5	−586.7	0.902	−585.8	−541.2	−586.7	0.903	−585.8	630[f]	
H	434.0	−0.027	434.0	438.4	−0.027	438.4	359.3	−0.032	359.2	435.4	359.3	−0.032	359.2	450[f]	397.1[k]
O	−5.718	0.099	−5.619	−9.740	0.050	−9.689	−4.492	−0.068	−4.560	−5.738	−4.492	−0.060	−4.561		
HSiS															
Si	−509.0	1.648	−507.3	−517.8	1.725	−516.1	−536.1	1.782	−534.3	−506.5	−536.0	1.792	−534.2		
H	328.0	−0.066	327.9	328.8	−0.070	328.8	269.1	−0.077	269.0	328.6	269.1	−0.078	269.0		304.9[k]
S	−0.105	0.048	−0.057	0.268	0.186	0.454	4.993	0.409	5.402	0.078	4.991	0.399	5.406		
SiOH															
O	−22.45	0.724	−21.73	−22.27	0.736	−21.53	−24.19	3.602	−20.59	−21.75	−23.97	3.616	−20.48		
Si	30.19	6.546	36.74	15.63	7.030	22.66	−2.347	27.41	25.06	37.87	−1.849	26.37	24.48		
H	54.72	−0.151	54.56	52.13	−0.149	51.98	53.17	−0.698	52.47	55.37	52.79	−0.877	52.11		51.3[k]
SiSH															
S	26.01	−0.164	25.85	21.34	−0.160	21.18	34.59	−0.256	34.34	26.03	34.57	−0.345	34.30		
Si	39.75	4.666	44.42	24.44	5.013	29.45	−0.616	7.816	7.200	44.21	−0.572	7.816	7.202		
H	131.8	−0.059	131.7	122.3	−0.058	122.2	114.5	−0.098	114.4	129.7	114.4	−0.099	114.3		109.6[k]
HgH															
Hg	7259	−189.7	7070	7708	−192.3	7516	9725	−221.8	9503	6989	9746	−333.5	9413	7002[g]	6357[l]
H	758.8	−1.800	757.0	742.0	−1.624	740.4	566.3	−1.909	564.4	728.4	543.5	−1.928	541.6	710[g]	
HgF															
Hg	18480	−22.76	18460	19870	−35.94	19830	20170	−25.55	20140	18420	20070	−63.06	20010	22163[h]	19292[l]
F	248.9	−144.8	104.2	299.3	−102.9	196.5	196.8	−183.9	12.91	87.57	188.0	−187.8	0.209	670[h]	
TiF_3															
Ti	−235.8	2.085	−233.7	−202.6	2.796	−199.8	−270.0	3.417	−266.6	−234.1	−269.9	3.435	−266.4	−184.8[i]	−260.8[m]
F	1.381	0.535	1.916	−18.53	0.597	−17.93	22.59	1.872	24.46	4.484	22.56	1.889	24.45	23.6[i]	26.1[m]

dx.doi.org/10.1021/ct200143w |J. Chem. Theory Comput. 2011, 7, 2175–2188

Table 1. Continued

	Spin-Polarized LR[b] (PBE)			Spin-Polarized LR[b] (PBE0)			Spin-Restricted LR[b] (PBE)			Spin-Polarized	Spin-Restricted EV[c]				
	FC+SD	PSOSO	total	FC+SD	PSOSO	total	FC+SD	PSOSO	total	EV	FC+SD	PSOSO	total	exp.	previous calc.
NpF_6[o]															
Np	−293.1	−2337	−2630	−19.20	−2541	−2560	5.948	−3398	−3392	−1437	47.94	479.2	527.1	−1994[l]	−2020[n]
F	−36.81	−10.33	−47.13	−50.71	−29.54	−80.25	0.000	−2.218	−2.218	−30.20	−1.770	8.723	22.90	−72.67[l]	−63[n]

[a] All calculations used a modified TZ2P basis set augmented by high-exponent functions added to all atoms (JCPL[43]). The point-nuclei approximation was used throughout. Where applicable, calculated coupling constants for symmetry-equivalent atoms have been averaged. [b] EV = expectation value approach ("first-order"). [c] LR = linear response approach ("second-order"). [d] Data taken from ref 45. [e] Data taken from ref 47. [f] Data taken from ref 49. [g] Data taken from ref 50. [h] Data taken from ref 51. [i] Data taken from ref 53. [j] Data taken from ref 46. [k] B3LYP/6-311++G**. Data taken from ref 48. [l] DKS2-RI. Data taken from ref 19. [m] Spin-restricted EV. Data taken from ref 13. [n] Dirac scattered-wave, first-order. Data taken from ref 52. [o] Six basis function combinations were removed because of linear dependency.

heaviest atom in our test set, neptunium, the isotropic coupling is predominantly caused by the PSOSO mechanism (~85% in the LR calculations). The results for NpF_6 somewhat resemble those that we obtained recently for the Δg-tensor of this complex,[11] in the sense that SO coupling treated at the LR perturbational level appears to be suitable for predicting the huge magnitude and the sign of its EPR parameters.

For most test compounds, calculations using the hybrid functional PBE0 yield results that are close to those obtained using the nonhybrid PBE functional. Again, larger deviations are confined to fluorine nuclei in the heavier compounds. For F in NpF_6, the hybrid DFT result agrees best with the experiment. For Np in NpF_6, the two functionals agree, in terms of the total isotropic coupling, but there are some differences regarding relative contributions of the FC+SD and PSOSO mechanisms. The calculations with PBE predict the FC+SD term to be ~10% of the total coupling, whereas in the calculation with the PBE0 functional, this mechanism becomes insignificant for Np.

The coupling constant calculated with the spin-restricted methods have a much wider variability than those calculated with other methods. While this approach seems fair for the medium atomic weight molecules in our test suite, it yields a vanishing hyperfine coupling for the simplest singlet radical that was tested with this method (CH_3). The planar geometry of CH_3, combined with the nature of the SOMO, is a typical case where spin polarization is essential to obtain the correct result. If the spin-restricted SOMO is a pure C 2p orbital perpendicular to the CH_3 plane, there cannot be any spin density at the carbon nucleus or at the hydrogen nuclei. As a result, the all-important contact term vanishes. The situation resembles that for the phenyl radical as discussed by Rieger.[3]

It is important to note that, when using spin-restricted orbitals, the sign of the isotropic coupling is fixed. That is, starting from a restricted set of orbitals and assigning the SOMO as one of the α orbitals always results in the $\rho^{\alpha-\beta}(0)$ term in eq 2 being positive. Some of the hyperfine couplings listed in Table 1 contain negative FC+SD contributions because of the negative magnetic moments for oxygen, silicon, and titanium nuclei. The spin-polarized calculations for CH_3 show that spin−polarization effects can be large enough to change the sign of the contact density at a nucleus away from the atom upon which an α spin SOMO is centered.

The calculations discussed up to this point used point charges for the nuclei. This approximation is not always suitable, especially when hyperfine properties for very heavy nuclei are considered. Indeed, Malkin et al. have reported sizable finite nucleus size effects calculated for hyperfine coupling constants of a set of Group 12 compounds including Hg, and for Group 11 atoms.[20] Spin-free relativistic DFT calculations using the Douglas−Kroll−Hess Hamiltonian and a Gaussian nuclear charge distribution yielded finite-nucleus effects that reduced the magnitude of Hg hyperfine coupling constants by as much as 20% relative to calculations using a point nucleus, with finite nucleus effects improving the agreement with experiment. Computations with a four-component relativistic method also showed reductions in calculated hyperfine coupling constants, in particular for mercury-containing compounds, although for other molecules the reduction was not as severe.[58]

Similar effects have also been investigated in ZORA computations of NMR spin−spin coupling (*J*-coupling), which involves perturbation operators that have the same r_N dependence as those that dominate the hyperfine coupling.[31] Finite nucleus

Table 2. Effect of the Finite-Nucleus Approximation on Calculated Hyperfine Coupling (Isotropic Couplings Given in MHz)[a]

	FC+SD		PSOSO		Total		
	point	finite	point	finite	point	finite	experimental
Nonhybrid (PBE)							
HgH							
Hg	7259	6677	−189.7	−190.5	7070	6487	7002[b]
H	758.8	758.9	−1.800	−1.793	757.0	757.1	710[b]
HgF							
Hg	18480	17180	−22.76	−21.32	18460	17160	22163[c]
F	248.9	250.6	−144.8	−146.8	104.2	103.8	670[c]
NpF_6[e]							
Np	−293.1	−216.8	−2337	−2338	−2630	−2555	−1994[d]
F	−36.81	−47.20	−10.33	−10.35	−47.13	−47.20	−72.67[d]
Hybrid (PBE0)							
HgH							
Hg	7708	7084	−192.3	−192.9	7516	6891	7002[b]
H	742.0	741.7	−1.624	−1.617	740.4	740.0	710[b]
HgF							
Hg	19870	18440	−35.94	−35.01	19830	18410	22163[c]
F	299.3	300.2	−102.9	−103.8	196.5	196.4	670[c]
NpF_6[e]							
Np	−19.20	13.40	−2541	−2543	−2560	−2530	−1994[d]
F	−50.71	−50.78	−29.54	−29.61	−80.25	−80.39	−72.67[d]

[a] A Gaussian nuclear charge distribution was used as described in ref 59 and section 2; otherwise, the computational protocol remained the same as previously described. [b] Data taken from ref 50. [c] Data taken from ref 51. [d] Data taken from ref 46. [e] Six basis function combinations removed due to linear dependency.

effects reduced the magnitude of one-bond Hg-ligand coupling constants typically by up to ∼10%. The correction terms arising from the finite nuclear volume have different origins: one is the modification of the electronic structure due to the weakened electrostatic electron−nucleus potential in the vicinity of the nuclear radius; the other one arises from the finite range of the nuclear current density in the perturbation operators, which is responsible for the nuclear magnetic moment. The level of treatment by a spherical Gaussian distribution may be considered relatively crude, yet the bulk of effects on isotropic hyperfine couplings (and NMR spin−spin coupling) is obtained with this straightforward-to-implement model and should be sufficient for computations of EPR parameters using DFT.

In order to investigate the magnitude of finite nucleus effects in the present LR ZORA hyperfine coupling calculations, we make a comparison between point nucleus and Gaussian nucleus calculations for HgH, HgF, and NpF_6. The results of these calculations are shown in Table 2. The finite nucleus correction decreases the magnitude of the isotropic hyperfine value for all molecules, but strongly so only for the heavy nuclei. In the PBE computations, as well as the PBE0 computations, the effect for Hg is an 8%−9% reduction of the isotropic coupling. The reduction is less pronounced than that which has been reported previously, but this is largely a consequence of the JCPL basis set not being able to reach a converged point-nucleus hyperfine coupling constant with respect to the augmentation of the basis with high exponent functions. This point has already been made in ref 31; therefore, we forego additional computations with basis sets that are more compatible with point nucleus computations. In previous work by Malkin et al. using Gaussian basis sets and the second-order Douglas−Kroll−Hess relativistic two-component Hamiltonian, the point nucleus Hg hyperfine couplings were larger than those in the experiment; therefore, finite nucleus effects improved the agreement with the experiment.[20] In our calculations, the trends for the finite nucleus corrections are the same, reducing the Hg hyperfine couplings. Because of the overall slightly lower magnitudes, the agreement with experiment deteriorates slightly when changing from point nuclei to finite nuclei. Ultimately, however, the performance of the computations should be assessed using the most realistic computational model which, for hyperfine coupling, should afford finite nuclei. Table 2 demonstrates that the finite nucleus model primarily affects the FC+SD mechanism, which is to be expected, given the "contact" nature of the FC operator. As a consequence, the hyperfine coupling for neptunium in NpF_6 is hardly affected by finite nucleus corrections because the hyperfine coupling is dominated by the PSOSO mechanism. In the PBE computations, where the FC+SD mechanism is not negligible for Np, a strong reduction (by ∼34%) of this mechanism due to finite nucleus effects is found. The JCPL basis used for Hg set represents an economic choice in terms of balancing accuracy and required computational resources. However, additional high-exponent functions may be needed to fully converge the finite nucleus results for Hg,[31] with respect to augmentation by high-exponent basis functions on Hg.

Additional computations were performed for HgF with basis sets of different flexibility. The results of varying basis set size with HgF are collected in Table 3. The series of basis sets is not designed to guarantee monotonous convergence but, instead, is used here to illustrate the variability of the results when using small, computationally efficient, basis sets (DZ, DZP), compared

Table 3. Effect of Basis Set Flexibility on the Calculated Calculated Isotropic Hyperfine Coupling Constants of HgF (Isotropic Couplings Given in MHz)[a]

	DZ	TZP	TZ2P	QZ4P	JCPL	TZ2P3[b]	experiment[c]
				Non-Hybrid (PBE)			
Hg							
FC+SD	14930	15390	15410	1704	17180	17510	
PSOSO	−15.01	−15.53	−13.57	−21.16	−21.32	−18.7	
total	14920	15370	15400	17020	17160	17490	22163
F							
FC+SD	−14.94	54.22	62.52	230.9	250.6	256.0	
PSOSO	−150.0	−146.8	−141.7	−146.1	−146.8	−143.7	
total	−165.0	−92.58	−79.21	84.87	103.8	112.3	670
				Hybrid (PBE0)			
Hg							
FC+SD	16070	16550	16620	18300	18440	18760	
PSOSO	−27.77	−30.30	−28.04	−34.77	−35.01	−31.80	
total	16040	16520	16600	18260	18410	18730	22163
F							
FC+SD	−0.650	101.4	108.8	273.5	300.2	307.5	
PSOSO	−104.4	−103.1	−100.3	−104.6	−103.8	−102.5	
total	−105.1	−1.686	8.467	168.9	196.4	205.0	670

[a] Computations with a Gaussian nuclear model. [b] TZ2P3 on Hg (see ref 31 and text for details); JCPL for F. [c] Experimental data taken from ref 51.

to basis sets that one may consider as being of good to very good quality (QZ4P and, to some extent, TZ2P). Regarding the convergence for high exponent augmentation, please see ref 31. Both JCPL and QZ4P have several high-exponent functions for Hg but only JCPL has exponents that significantly exceed the nuclear charge for F. Therefore, the effect from the high-exponent augmentation is more strongly seen in the FC+SD contributions of the F hyperfine coupling. For Hg, the JCPL and QZ4P results are more similar, relative to the magnitude of the FC+SD term. Across the table, there is a readily apparent trend for the FC+SD mechanism: increasing the number of basis functions increases the FC+SD contribution, better matching experiment. The sensitivity of the FC mechanism and its relativistic generalizations in nuclear spin−spin coupling is well-documented[7,60,61] and also is seen here to affect the hyperfine coupling significantly. Table 3 affords additional results with a Hg basis of higher augmentation (TZ2P3), affording Slater exponents of up to 4×10^4 but otherwise comparable to JCPL, which was previously used for a *J*-coupling benchmark.[31] Compared to the JCPL basis, which is limited to exponents up to 1×10^4, there is a slight increase in the Hg hyperfine couplings, but not sufficient to obtain quantitative agreement with the experiment. We observe an effect on the F hyperfine couplings when comparing JCPL and TZ2P3, showing that an improved description of the Hg valence orbitals core tails is coupled to changes in the outer region of these orbitals as well. The coupling for fluorine in HgF, although showing some improvement with the larger basis sets, remains conspicuously underestimated, compared to experiment. According to Table 1, with the PBE functional, the comparison of the LR approach with the EV approach reveals some shortcomings of the LR approach for the linear HgF molecule, but not to an extent that would indicate a severe breakdown of the LR calculations. There is a strong cancellation between the FC+SD and the PSOSO mechanisms for fluorine. Such a balance of opposing terms tends to expose deficiencies in the computational model. We tentatively attribute the discrepancy between the calculated and the experimental fluorine hyperfine coupling for HgF to approximations in the density functionals preventing an accurate description of the spin density distribution and its linear response in this system.

4.2. Paramagnetic NMR Effects in Some Ru(III) Complexes. Knowledge of the hyperfine tensor can be used in the prediction and analysis of paramagnetic NMR shifts.[4,8,62,63] The contact shift due to the hyperfine interaction is, to a first approximation, given by[64,65]

$$\delta^{\mathrm{FC}} = \frac{g_{\mathrm{iso}}\beta_e}{g_N\beta_N}\frac{S(S+1)}{3kT}A_{\mathrm{iso}} \qquad (21)$$

where g_{iso} is the isotropic average of the *g*-tensor. Because of this dependence on the *g*-tensor, prediction of pNMR shifts is not straightforward, as the dependence of the pNMR shift on excess α or β electron spin density at a nucleus is to be combined with the sign and magnitude of g_{iso}. For a given calculated sign of A_{iso}, it is possible for the contribution to pNMR shift to be of the opposite sign if the value of g_{iso} is negative. This situation is not typically encountered for organic radicals, but it may well be the case for complexes that contain heavy elements.

In a previous study, Rastrelli and Bagno investigated the effect of relativistic effects in calculations of ligand pNMR shifts of several Ru(III) compounds of potential pharmaceutical interest, with particular emphasis placed on the contribution of contact shifts to the overall pNMR shifts.[22] As a first application of our new LR ZORA method for computations of hyperfine tensors, calculations were carried out for three complexes selected from the test set of Rastrelli and Bagno: NAMI, $Ru(acac)_3$, and $Ru(tfac)_3$, whose structures are shown in Figure 1. Because the isotropic *g*-factor plays a role (as seen in eq 21), *g*-tensors were calculated using a compatible ZORA method (i.e., first-order EV *g*-tensors were combined with EV hyperfine tensor calculations,

and LR *g*-tensors were combined with LR hyperfine tensor calculations).

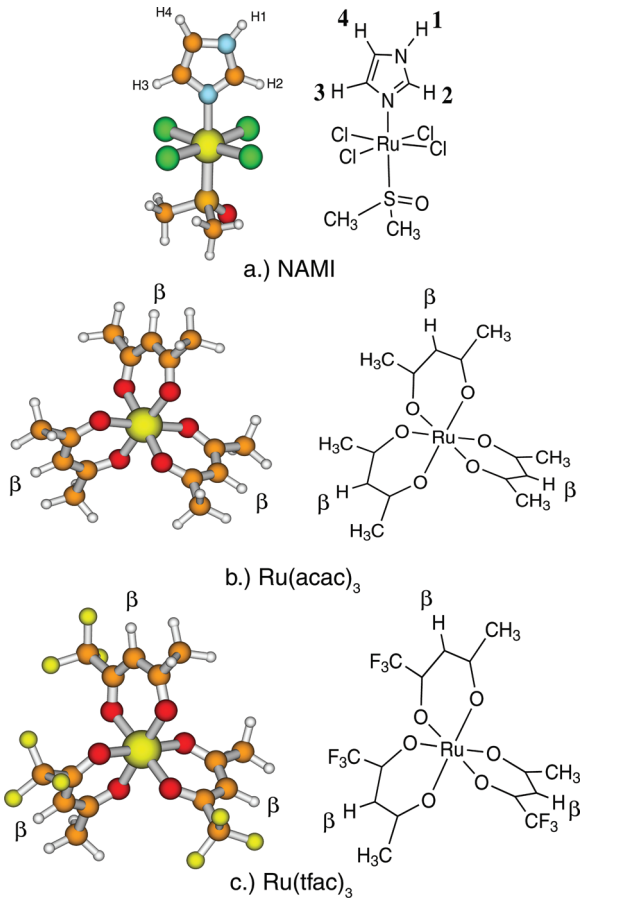

Figure 1. Structures selected from the Rastrelli and Bagno ruthenium complex benchmark set. See ref 22.

In Table 4, calculated isotropic hyperfine couplings and isotropic *g*-factors are collected and compared with data previously reported by Rastrelli and Bagno. All calculations that employ a relativistic Hamiltonian are seen to yield quite comparable results, with very little deviation among the *g*-tensors and only slight variations in the isotropic hyperfine couplings. The differences in the hyperfine couplings are likely a consequence of the use of the JCPL basis for the protons, as opposed to the universal use of the TZ2P basis by Rastrelli and Bagno. Comparison between the nonhybrid functionals BP86 and PBE shows almost negligible differences with regard to both EV and LR approaches. At the relativistic level, switching to a hybrid functional shows a tendency to increase both the hyperfine coupling magnitudes (with some notable exceptions) as well as the isotropic *g*-factors. The effects from switching to the hybrid are noticeable but not dramatic for the three Ru(III) complexes.

Table 5 lists the pNMR contact shifts predicted from eq 21, based on the calculated isotropic hyperfine and *g*-tensor data of Table 4. There is generally good agreement in both magnitude and sign among all relativistic methods, with the main exception being the H2 proton of NAMI. Overall, the comparison with the experiment was not quantitative in ref 22, but the overall trends for the set of complexes were reproduced. Because of the smaller benchmark set used here to test the new implementation, we forego a discussion of the chemical shifts and refer the reader to ref 22. In agreement with Rastrelli and Bagno, the calculated contact shifts do not seem to be negative enough for the H2−H4 and NH protons of NAMI to bring the sign of the overall calculated and experimental chemical shifts for these protons to agreement. The calculated contact shifts for $Ru(acac)_3$ and $Ru(tfac)_3$ are large enough such that the sign of the overall calculated chemical shifts match the experiment, but the magnitude of the contact shifts are too large for the methyl protons.

Knowledge of the hyperfine tensor, along with the *g*-tensor, can also be used in the prediction of pNMR pseudo-contact (PC)

Table 4. Isotropic Hyperfine Couplings and *g*-Factors Calculated for the Present Work and Comparison with Data from Rastrelli and Bagno[22] [a]

	Rastrelli and Bagno[22]		EV[d]		LR[e]		
	Non-Rel.[b]	Rel.[c]	(PBE)	(BP86)	(PBE)	(BP86)	(B3LYP)
NAMI							
g_{iso}	1.858	2.194	2.193	2.193	2.203	2.203	2.233
CH_3	−0.20	−0.32	−0.316	−0.307	−0.327	−0.323	−0.336
H2	0.08	0.094	0.123	0.128	−0.034	−0.019	−0.049
H3	−0.03	−0.11	−0.067	−0.067	−0.188	−0.234	−0.186
H4	−0.10	−0.15	−0.142	−0.145	−0.142	−0.143	−0.163
NH1	−0.06	−0.072	−0.063	−0.062	−0.070	−0.074	−0.102
$Ru(acac)_3$							
g_{iso}	2.683	2.138	2.103	2.102	2.123	2.122	2.237
CH_3	−0.54	−0.59	−0.676	−0.709	−0.669	−0.711	−0.726
H-β	−0.68	−0.87	−1.382	−1.557	−1.436	−1.595	−1.286
$Ru(tfac)_3$							
g_{iso}	2.587	2.084	2.082	2.082	2.103	2.102	2.209
CH_3	−0.81	−0.89	−0.693	−0.792	−0.702	−0.744	−0.828
H-β	−1.50	−1.87	−1.617	−1.846	−1.730	−1.899	−1.586

[a] Isotropic *g*-factors were calculated using a method equivalent to that used in the calculation of the hyperfine tensor. [b] Hyperfine couplings in MHz. Gaussian09/B3LYP with cc-pVTZ on H,C,N,O,S,F,Cl and DZVP on Ru. [c] ADF/EV/BP86/TZ2P. [d] EV = expectation value approach ("first-order"). [e] LR = linear response approach ("second-order").

Table 5. Comparison of pNMR Contact Shifts for the Ru(III) Complexes of Figure *1* Estimated from eq 21, Using the Data from Table 4[a]

	Rastrelli and Bagno[22]		EV[d]		LR[e]		
	Non-Rel.[b]	Rel.[c]	PBE	BP86	PBE	BP86	B3LYP
NAMI[f]							
CH_3	−6.25	−9.41	−9.166	−8.905	−9.513	−9.412	−9.914
H2	2.45	2.73	3.580	3.726	−0.991	−0.554	−1.447
H3	−0.98	−3.21	−1.954	−1.955	−5.478	−6.818	−5.494
H4	−3.29	−4.29	−4.107	−4.219	−4.138	−4.167	−4.814
NH1	−1.99	−2.11	−1.820	−1.793	−2.040	−2.156	−3.013
Ru(acac)$_3$[g]							
CH_3	−19.3	−16.8	−18.36	−19.27	−18.35	−19.50	−21.00
H-β	−24.2	−24.6	−37.56	−42.32	−39.39	−43.75	−37.19
Ru(tfac)$_3$[h]							
CH_3	−25.4	−24.7	−18.85	−21.53	−19.26	−20.43	−23.86
H-β	−46.7	−51.5	−43.96	−50.17	−47.50	−52.12	−45.72

[a] Physical constants used in eq 21 are those reported in ref 66. [b] Gaussian09/B3LYP with cc-pVTZ on H,C,N,O,S,F,Cl and DZVP on Ru. [c] ADF/EV/BP86/TZ2P. [d] EV = expectation value approach ("first-order"). [e] LR = linear response approach ("second-order"). [f] Data obtained at 25 °C. [g] Data obtained at 32 °C. [h] Data obtained at 29 °C. See ref 22.

shifts. An approach for calculating the isotropic PC contribution was previously derived by McConnell and Robertson,[67] expanded upon by Kurland and McGarvey,[65] and discussed in detail by Bertini et al.[33] This approach approximates the paramagnetic center as a point similar to eq 13. The overall PC shift resulting from the point approximation may take many forms, including[33]

$$\delta^{\mathrm{pcs}} = \frac{1}{12\pi r^5}\mathrm{Tr}\{3\mathbf{r} \otimes (\mathbf{r}\cdot\boldsymbol{\chi}) - r^2\boldsymbol{\chi}\} \tag{22a}$$

$$\delta^{\mathrm{pcs}} = \frac{1}{4\pi r^3}\left[(\chi_{zz} - \overline{\chi})\frac{2z^2 - x^2 - y^2}{2r^2} + (\chi_{xx} - \chi_{yy})\frac{x^2 - y^2}{2r^2} + \chi_{xy}\frac{2xy}{r^2} + \chi_{xz}\frac{2xz}{r^2} + \chi_{yz}\frac{2yz}{r^2}\right] \tag{22b}$$

$$\delta^{\mathrm{pcs}} = \frac{1}{4\pi r^3}\left[(\chi_{zz} - \overline{\chi})\frac{3\cos^2\theta - 1}{2} + (\chi_{xx} - \chi_{yy})\frac{\sin^2\theta\cos 2\phi}{2} + \chi_{xy}\sin^2\theta\sin 2\phi + \chi_{xz}\sin 2\theta\cos\phi + \chi_{yz}\sin 2\theta\sin\phi\right] \tag{22c}$$

where $\mathbf{r}$ is the vector from the paramagnetic center to the NMR nucleus of interest, r is the distance $|\mathbf{r}|$, and θ and ϕ are polar angles with respect to the principal axes. The principal components of the magnetic susceptibility tensor χ can be obtained using the principal elements of the g-tensor:[33]

$$\chi_{ii} = \mu_0\beta_e^{\,2}g_{ii}^{\,2}\frac{S(S+1)}{3kT} \tag{23}$$

An alternate approach to calculating PC shifts that arises from a rigorous derivation of paramagnetic NMR shielding tensors previously carried out by Moon and Patchkovskii,[8] and shown by Hrobárik et al. to be applicable to metal complexes,[62] does not make particular assumptions about the spatial distribution of the spin density from which the dipolar hyperfine tensor is calculated. The PC shift can be calculated in such a way by

$$\delta^{\mathrm{pcs}} = \frac{\beta_e}{\beta_N g_N}\frac{S(S+1)}{9kT}\mathrm{Tr}[\mathrm{g}\mathbb{A}_{\mathrm{dip}}^{\mathrm{T}}] \tag{24}$$

with all constants given in SI units, and the traceless dipolar hyperfine tensor $\mathbb{A}_{\mathrm{dip}} = \mathbb{A} - A_{\mathrm{iso}}\mathbb{1}$ with A_{iso} being the isotropic value of the hyperfine tensor, and $\mathbb{1}$ being a 3×3 identity matrix. The superscript T denotes a transpose. Because of the symmetry of the g-tensor, eq 24 can be written in several equivalent forms, differing in the order of $\mathrm{g}\mathbb{A}_{\mathrm{dip}}$ matrix multiplication and whether or not the transpose of $\mathbb{A}_{\mathrm{dip}}$ is used. Hrobárik et al. obtained an equivalent expression for the PC shift.[62] We adopt the coordinate frame used by Moon and Patchkovskii,[8] where the g-tensor is diagonal and the A-tensor is transformed to the principal axis system (PAS) of the g-tensor. The $\mathbb{A}_{\mathrm{dip}}$ tensor (given in SI units of Joules) can be approximated in the same way as in the derivation leading up to eq 13, or alternatively, from the Hamiltonian expression for interacting magnetic dipoles:

$$\hat{H} = -\frac{\mu_0}{4\pi}\left[\frac{3(\boldsymbol{\mu}_N\cdot\mathbf{r})(\boldsymbol{\mu}_e\cdot\mathbf{r})}{r^5} - \frac{\boldsymbol{\mu}_N\cdot\boldsymbol{\mu}_e}{r^3}\right] \tag{25}$$

$$= \frac{\mu_0}{4\pi}g_e\beta_e g_N\beta_N\left[\frac{3(\mathbf{I}\cdot\mathbf{r})(\mathbf{I}\cdot\mathbf{r})}{r^5} - \frac{\mathbf{I}\cdot\mathbf{S}}{r^3}\right] \tag{26}$$

where $\boldsymbol{\mu}_N$ is the nuclear magnetic moment operator ($\boldsymbol{\mu}_N = \gamma_N\mathbf{I} = g_N\beta_N\mathbf{I}$) and $\boldsymbol{\mu}_e$ is the magnetic moment for the electron. In eq 26, the magnetic moment of a free electron ($\boldsymbol{\mu}_e = -g_e\beta_e\mathbf{S}$) was used, and, under this approximation, the resulting equation for the traceless dipolar hyperfine tensor is identical to eq 13 (given here in SI units):

$$A_{u,v}^{\mathrm{dip}} \approx \frac{\mu_0}{4\pi}g_e\beta_e g_N\beta_N\left[3\frac{r_{N,u}r_{N,v}}{{r_N}^5} - \frac{\delta_{uv}}{{r_N}^3}\right] \tag{27}$$

In molecules that contain heavy elements, particularly transition metals, such an approximation is likely not valid and a better

Table 6. Comparison of eq 22a and eq 24 in Calculating Pseudo-contact Shifts in Selected Ru(III) Complexes[a]

	Chemical Shift (ppm)	
	eq 22a[33]	eq 24
NAMI[b]		
CH_3	−2.31	−1.41
H2	−3.52	−2.09
H3	−4.51	−2.30
H4	−2.19	−0.98
NH1	−2.23	−0.99
Ru(acac)$_3$ [c]		
CH_3	−0.09	−0.04
H-β	−1.05	−1.25
Ru(tfac)$_3$ [d]		
CH_3	−0.09	−0.04
H-β	−0.97	−1.17

[a] PBE computations. [b] Data obtained at 25 °C. [c] Data obtained at 32 °C. [d] Data obtained at 29 °C.

expression for the electron spin magnetic moment is $\boldsymbol{\mu}_e = -\beta_e \mathbb{g}\mathbf{S}$, where $\mathbb{g}$ is the full g-tensor.[1] By substituting this into eq 25, one can obtain an expression for the dipolar hyperfine tensor:

$$\mathbb{A}_{\mathrm{dip}} \approx \left(\frac{\mu_0 \beta_e g_N \beta_N}{4\pi}\right) \mathbb{T} \cdot \mathbb{g} \qquad (28)$$

where $\mathbb{T} = r^{-5}[3\mathbb{r}\mathbb{r} - r^2\mathbb{1}]$ is the geometric factor seen in eqs 13 and 27; this is consistent with McConnell and Robertson's derivation.[67] Substituting eq 28 into eq 24 results in the equations given by Bertini et al. (eqs 22a−22c),[33] assuming diagonal g and magnetic susceptibility tensors.

To compare the two approaches, the isotropic PC shifts were calculated for the Ru(III) complexes of the Rastrelli and Bagno study discussed above. The results are collected in Table 6. The calculated g-tensor was diagonalized and both the approximate hyperfine tensor calculated using eq 24 and the tensor from the ZORA DFT calculations were transformed to the PAS of $\mathbb{g}$ accordingly. The conversion factor used for the calculated ZORA hyperfine tensor uses g_e. Therefore, in order to directly compare the two approaches, the hyperfine tensor from ADF was first divided by the value of g_e, and then multiplied by the calculated g-tensor in order to arrive at eq 28.

The agreement between the two methods reveals some significant differences. However, there is universal agreement in sign. (See the Supporting Information for more detailed data.) The discrepancies between the two methods must be attributed to the point-dipole approximation underlying eq 22a, which is not used in the PC shifts calculated from eq 24. Visualization of the SOMOs for the Ru(III) complexes (see the Supporting Information) demonstrates that these orbitals have a significant spatial extension; thus, an approximation that neglects the spatial distribution of the spin density can be expected to break down to some extent. The PC shifts calculated from the full ZORA DFT hyperfine tensors (eq 24) are in most cases smaller in magnitude than those calculated with the point-dipole approximation. Qualitatively, the situation is similar to where one considers the difference of the electrostatic energy between two point charges and the interaction between a point charge and a continuous spherical charge distribution, with the latter being smaller in magnitude. The most noticeable discrepancies are found with the H-β protons on Ru(acac)$_3$ and Ru(tfac)$_3$. Two of these protons on each complex are bonded to carbon atoms that contain significant electron density from the SOMO. Considering the spatial distribution of the spin density in the hyperfine tensor computations results in a sizable increase of calculated PC shift magnitudes for Ru(acac)$_3$, and a slightly smaller (but still significant) increase with the corresponding protons in Ru(tfac)$_3$. The other H-β protons, which lie along the principal axis of their respective complexes, do not afford SOMO density on the adjacent carbons; therefore, the effect is not as large.

Therefore, the trend is that the spatial extension of the SOMO, compared to a point spin density, will yield a smaller PC shift, potentially excluding cases where the SOMO is significantly delocalized to regions near the nucleus for which the PC shift is being calculated.

Isosurface plots of the SOMOs and tables with individual proton contact and PC shifts are available in the Supporting Information.

5. SUMMARY AND OUTLOOK

A density functional theory (DFT)-based method for calculating the electron paramagnetic resonance hyperfine coupling tensors, using second-order perturbation theory and the relativistic zeroth-order regular approximation (ZORA) Hamiltonian, has been developed and tested for radicals with few atoms and for three Ru(III) complexes. The implementation (1) makes use of Slater-type orbital (STO) basis sets, (2) is capable of both nonhybrid and hybrid DFT computations, and (3) supports a Gaussian finite nucleus model. The new procedure performs well, compared to hyperfine couplings calculated using an expectation value (first-order) approach developed previously by van Lenthe et al.[13] Using a hybrid functional shows a tendency to increase the magnitude of the calculated hyperfine couplings. The use of a finite nucleus model may significantly improve the agreement with the experiment for very heavy atoms. The role of basis set was also investigated, with the requirement for high-exponent basis functions to describe the core electronic structure along with flexibility in the valence region being illustrated in computations on HgF. Preliminary test calculations of contact and pseudo-contact paramagnetic NMR chemical shifts based on calculated hyperfine and g-tensors for a set of Ru(III) complexes demonstrate that the method is computationally efficient.

■ ASSOCIATED CONTENT

Supporting Information. Supporting Information is available containing information about individual proton shifts and SOMO distribution for the Ru(III) complexes. This information is available free of charge via the Internet at http://pubs.acs.org.

■ AUTHOR INFORMATION

Corresponding Author
*E-mail: jochena@buffalo.edu.

■ ACKNOWLEDGMENT

The authors acknowledge support of this research from the Center of Computational Research at SUNY Buffalo, and

financial support from the U.S. Department of Energy (Grant No. DE-SC0001136) (BES Heavy Element Chemistry Program).

REFERENCES

(1) Atherton, N. M. *Ellis Horwood Series in Physical Chemistry*; Ellis Horwood, PTR Prentice Hall: New York, 1993; pp 46−50, 210.

(2) Eriksson, L. A. ESR Hyperfine Calculations. In *Encyclopedia of Computational Chemistry*; Schleyer, P. v. R., Ed.; Wiley: Chichester, U.K., 1998; pp 952−958.

(3) Rieger, P. H. *Electron Spin Resonance. Analysis and Interpretation*; The Royal Society of Chemistry: Cambridge, U.K., 2007; p 3.

(4) Abragam, A.; Bleaney, B. *Electron Paramagnetic Resonance of Transition Ions*; Clarendon Press: Oxford, U.K., 1970; pp 133−216.

(5) Pyykkö, P. *Theor. Chem. Acc.* **2000**, *103*, 214–216.

(6) Kossmann, S.; Kirchner, B.; Neese, F. *Mol. Phys.* **2007**, *105*, 2049–2071.

(7) Autschbach, J.; Zheng, S. *Annu. Rep. NMR Spectrosc.* **2009**, *67*, 1–95.

(8) Moon, S.; Patchkovskii, S. First-principles calculations of paramagnetic NMR shifts. In *Calculation of NMR and EPR Parameters. Theory and Applications*; Kaupp, M., Bühl, M., Malkin, V. G., Eds.; Wiley−VCH: Weinheim, Germany, 2004.

(9) Rastrelli, F.; Bagno, A. *Chem.—Eur. J.* **2009**, *15*, 7990–8004.

(10) Arbuznikov, A. V.; Vaara, J.; Kaupp, M. *J. Chem. Phys.* **2004**, *120*, 2127–2139.

(11) Autschbach, J.; Pritchard, B. *Theor. Chem. Acc.* **2011**, *129*, 453−466.

(12) van Lenthe, E.; Baerends, E. J.; Snijders, J. G. *J. Chem. Phys.* **1993**, *99*, 4597–4610.

(13) van Lenthe, E.; van der Avoird, A.; Wormer, P. E. S. *J. Chem. Phys.* **1998**, *108*, 4783–4796.

(14) Barone, V.; Cimino, P.; Stendardo, E. *J. Chem. Theor. Comput.* **2008**, *4*, 751–764.

(15) Neese, F. *Coord. Chem. Rev.* **2009**, *253*, 526–563.

(16) Hermosilla, L.; Calle, P.; Garca de la Vega, J. M.; Sieiro, C. *J. Phys. Chem. A* **2005**, *109*, 1114–1124.

(17) Hermosilla, L.; Calle, P.; Garca de la Vega, J. M.; Sieiro, C. *J. Phys. Chem. A* **2005**, *109*, 7626–7635.

(18) Remenyi, C.; Reviakine, R.; Arbuznikov, A. V.; Vaara, J.; Kaupp, M. *J. Phys. Chem. A* **2004**, *108*, 5026–5033.

(19) Komorovský, S.; Repiský, M.; Malkina, O. L.; Malkin, V. G.; Malkin, I.; Kaupp, M. *J. Chem. Phys.* **2006**, *124*, 084108.

(20) Malkin, E.; Malkin, I.; Malkina, O. L.; Malkin, V. G.; Kaupp, M. *Phys. Chem. Chem. Phys.* **2006**, *8*, 4079–4085.

(21) Baerends, E. J.; Ziegler, T.; Autschbach, J.; Bashford, D.; Bérces, A.; Bickelhaupt, F. M.; Bo, C.; Boerrigter, P. M.; Cavallo, L.; Chong, D. P.; Deng, L.; Dickson, R. M.; Ellis, D. E.; van Faassen, M.; Fan, L.; Fischer, T. H.; Fonseca Guerra, C.; Ghysels, A.; Giammona, A.; van Gisbergen, S. J. A.; Götz, A. W.; Groeneveld, J. A.; Gritsenko, O. V.; Grüning, M.; Gusarov, S.; Harris, F. E.; van den Hoek, P.; Jacob, C. R.; Jacobsen, H.; Jensen, L.; Kaminski, J. W.; van Kessel, G.; Kootstra, F.; Kovalenko, A.; Krykunov, M. V.; van Lenthe, E.; McCormack, D. A.; Michalak, A.; Mitoraj, M.; Neugebauer, J.; Nicu, V. P.; Noodleman, L.; Osinga, V. P.; Patchkovskii, S.; Philipsen, P. H. T.; Post, D.; Pye, C. C.; Ravenek, W.; Rodríguez, J. I.; Ros, P.; Schipper, P. R. T.; Schreckenbach, G.; Seldenthuis, J. S.; Seth, M.; Snijders, J. G.; Solà, M.; Swart, M.; Swerhone, D.; te Velde, G.; Vernooijs, P.; Versluis, L.; Visscher, L.; Visser, O.; Wang, F.; Wesolowski, T. A.; van Wezenbeek, E. M.; Wiesenekker, G.; Wolff, S. K.; Woo, T. K.; Yakovlev, A. L. Amsterdam Density Functional; SCM, Theoretical Chemistry, Scientific Computing & Modelling (SCM), Theoretical Chemistry, Vrije Universiteit: Amsterdam, The Netherlands. (URL: http://www.scm.com.)

(22) Rastrelli, F.; Bagno, A. *Magn. Reson. Chem.*. **2010**, *48* (S1), S132−S141.

(23) Philipsen, P. H. T.; van Lenthe, E.; Snijders, J. G.; Baerends, E. J. *Phys. Rev. B* **1997**, *56*, 13556–13562.

(24) Nichols, P.; Govind, N.; Bylaska, E. J.; de Jong, W. A. *J. Chem. Theor. Comput.* **2009**, *5*, 491–499.

(25) Aquino, F.; Govind, N.; Autschbach, J. *J. Chem. Theor. Comput.* **2010**, *6*, 2669–2686.

(26) van Wüllen, C. *J. Chem. Phys.* **1998**, *109*, 392–399.

(27) Patchkovskii, S.; Strong, R. T.; Pickard, C. J.; Un, S. *J. Chem. Phys.* **2005**, *122*, 214101.

(28) Autschbach, J.; Ziegler, T. *J. Chem. Phys.* **2000**, *113*, 9410–9418.

(29) Autschbach, J.; Ziegler, T. *J. Chem. Phys.* **2000**, *113*, 936–947.

(30) Autschbach, J. *J. Chem. Phys.* **2008**, *129*, 094105 (and erratum, *J. Chem. Phys*. **2009**, *130*, 209901).

(31) Autschbach, J. *ChemPhysChem* **2009**, *10*, 2274–2283.

(32) Schreckenbach, G.; Ziegler, T. *J. Phys. Chem. A* **1997**, *101*, 3388–3399.

(33) Bertini, I.; Luchinat, C.; Parigi, G. *Prog. Nucl. Magn. Reson. Spectrosc.* **2002**, *40*, 249–273.

(34) Visscher, L.; Dyall, K. *At. Data Nucl. Data Tables* **1997**, *67*, 207–224.

(35) Andrae, D. *Phys. Rep* **2000**, *336*, 413–527.

(36) Becke, A. D. *Phys. Rev. A* **1988**, *38*, 3098–3100.

(37) Perdew, J. P. *Phys. Rev. B* **1986**, *33*, 8822–8824.

(38) Perdew, J. P. *Phys. Rev. B* **1986**, *34*, 7406.

(39) Ernzerhof, M.; Scuseria, G. E. *J. Chem. Phys.* **1999**, *110*, 5029–5036.

(40) Adamo, C.; Barone, V. *J. Chem. Phys.* **1999**, *110*, 6158–6170.

(41) Watson, M. A.; Handy, N. C.; Cohen, A. J.; Helgaker, T. *J. Chem. Phys.* **2004**, *120*, 7252–7261.

(42) Bryce, D.; Autschbach, J. *Can. J. Chem.* **2009**, *87*, 927–941.

(43) Moncho, S.; Autschbach, J. *J. Chem. Theor. Comput.* **2010**, *6*, 223–234.

(44) Becke, A. D. *J. Chem. Phys.* **1993**, *98*, 5648–5652.

(45) Weltner, Jr., W. *Magnetic Atoms and Molecules*; Dover Publications, Inc.: New York, 1983.

(46) Butler, J. E.; Hutchison, C. A., Jr. *J. Chem. Phys.* **1981**, *74*, 3102–3119.

(47) Holmberg, R. W. *J. Chem. Phys.* **1969**, *51*, 3255–3260.

(48) Grein, F. *Chem. Phys.* **2004**, *296*, 71–78.

(49) Van Zee, R. J.; Ferrante, R. F.; Weltner, W., Jr. *J. Chem. Phys.* **1985**, *83*, 6181–6187.

(50) Knight, L. B., Jr.; Weltner, W., Jr. *J. Chem. Phys.* **1971**, *55*, 2061–2070.

(51) Knight, L. B., Jr.; Fisher, T. A.; Wise, M. B. *J. Chem. Phys.* **1981**, *74*, 6009–6013.

(52) Case, D. A. *J. Chem. Phys.* **1985**, *83*, 5792–5796.

(53) De Vore, T. C.; Weltner, W. *J. Am. Chem. Soc.* **1977**, *99*, 4700–4703.

(54) Belanzoni, P.; van Lenthe, E.; Baerends, E. J. *J. Chem. Phys.* **2001**, *114*, 4421–4433.

(55) Patchkovskii, S.; Schreckenbach, G. Calculation of EPR g-tensors with density functional theory. In *Calculation of NMR and EPR Parameters. Theory and Applications*; Kaupp, M., Bühl, M., Malkin, V. G., Eds.; Wiley−VCH: Weinheim, Germany, 2004.

(56) Malkina, O. L.; Salahub, D. R.; Malkin, V. G. *J. Chem. Phys.* **1996**, *105*, 8793–8800.

(57) Malkin, V. G.; Malkina, O. L.; Salahub, D. R. *Chem. Phys. Lett.* **1994**, *221*, 91–99.

(58) Malkin, E.; Repiský, M.; Komorovský, S.; Mach, P.; Malkina, O. L.; Malkin, V. G. *J. Chem. Phys.* **2011**, *134*, 044111.

(59) Hansen, J.; Autschbach, J.; Davies, H. *J. Org. Chem.* **2009**, *74*, 6555–6563.

(60) Kowalewski, J. *Annu. Rep. NMR Spectrosc.* **1982**, *12*, 81–176.

(61) Helgaker, T.; Jaszuński, M.; Ruud, K. *Chem. Rev.* **1999**, *99*, 293–352.

(62) Hrobárik, P.; Reviakine, R.; Arbuznikov, A. V.; Malkina, O. L.; Malkin, V. G.; Köhler, F. H.; Kaupp, M. *J. Chem. Phys.* **2007**, *126*, 024107.

(63) Kaupp, M.; Köhler, F. H. *Coord. Chem. Rev.* **2009**, *253*, 2376–2386.

(64) Vega, A. J.; Fiat, D. *Pure Appl. Chem.* **1972**, *32*, 307–315.

(65) Kurland, R. J.; McGarvey, B. R. *J. Magn. Reson.* **1970**, *2*, 286–301.
(66) Mohr, P. J.; Taylor, B. N.; Newell, D. B. *Rev. Mod. Phys.* **2008**, *80*, 633–730.
(67) McConnell, H. M.; Robertson, R. E. *J. Chem. Phys.* **1958**, *29*, 1361–1365.